Published in final edited form as:
Nanoscale. 2012 February 7; 4(3): 715–726. doi:10.1039/c2nr11562j.

Single nanoparticle detectors for biological applications

Abdulkadir Yurt[a], **George G. Daaboul**[b], **John H. Connor**[c], **Bennett B. Goldberg**[a,b,d,e], and **M. Selim Ünlü**[a,b,d,e]

Abdulkadir Yurt: yurt@bu.edu; George G. Daaboul: gdaa1987@bu.edu; John H. Connor: jhconnor@bu.edu; Bennett B. Goldberg: goldberg@bu.edu; M. Selim Ünlü: selim@bu.edu

[a]Division of Materials Science and Engineering, Boston University, Boston, MA, 02215, USA

[b]Biomedical Engineering Department, Boston University, Boston, MA, 02215, USA

[c]Physics Department, Boston University, Boston, MA, 02215, USA

[d]Department of Microbiology, Boston University School of Medicine, Boston, MA, 02118, USA

[e]Electrical and Computer Engineering Department, Boston University, Boston, MA, 02215, USA

Abstract

Nanoparticle research has become increasingly important in the context of bioscience and biotechnology. Practical use of nanoparticles in biology has significantly advanced our understanding about biological processes in the nanoscale as well as led to many novel diagnostic and therapeutic applications. Besides, synthetic and natural nanoparticles are of concern for their potential adverse effect on human health. Development of novel detection and characterization tools for nanoparticles will impact a broad range of disciplines in biological research from nanomedicine to nanotoxicology. In this article, we discuss the recent progress and future directions in the area of single nanoparticle detectors with an emphasis on their biological applications. A brief critical overview of electrical and mechanical detection techniques is given and a more in-depth discussion of label-free optical detection techniques is presented.

1 Introduction

Synthetic nanoparticles have drastically impacted bioscience and biotechnology in the last decade.[1–5] Semiconductor, metal, carbon and polymer based nanoparticles have found many biological applications: labeling in diagnostic bioimaging[6,7] and biosensing,[8,9] agents for drug delivery,[10] and cancer treatment,[11,12] to name a few. The growing use of the synthetic nanoparticles in industrial products such as cosmetics, processed food, drugs, *etc*. has raised serious concerns about potential toxic effects of nanoparticles on human health.[13–15] For example, inhaled nanoparticles can cross the air–blood barrier and accumulate in tissues causing inheritable mutations.[16] Individual nanoparticles can also alter the normal routine of a biological system by aggregating proteins on their surfaces and forming protein coronas.[17,18] While the safety evaluation of a bulk material typically involves dose, chemical composition and exposure route, many more factors determine the safety grade of a nanoparticle including size, shape, adsorbability and charge.[19] A variety of the factors contributing to the toxicity assessment require significant effort to understand the full extent of the effects of the nanoparticles on the biological systems.

Correspondence to: M. Selim Ünlü, selim@bu.edu.

Various natural nanoparticles such as small pathogens are a serious threat to human health. Every year, millions of people die worldwide due to viral infectious diseases.[20] It has been shown that viruses are an established cause of a variety of human cancers[21–23] including rare and common types such as Merkel cell carcinoma[24] and liver cancer,[25] respectively. Moreover, infectious viruses may pose substantial security threats towards societies as they cause deadly epidemics[26] and can potentially be employed in biological weapons.[27,28]

The detection and characterization of nanoparticles in the single particle limit bear utmost importance for understanding and preventing the negative consequences of the nanoparticles as well as developing devices for diagnostic and therapeutic applications. This necessity has spurred a surge in developing novel methods for single nanoparticle characterization in the last decade.[29–31] Despite the significant progress, nanoparticle detection still remains a challenge for most practical applications. For instance, the real-life scenarios typically require detection of nanoparticles in an inhomogeneous solution containing other particles with different sizes, shapes and chemical constituents. Therefore, the heterogeneous properties of the sample require specific detection mechanisms to be able to classify the nanoparticles of interest in a complex population. Moreover, the throughput/speed and reliability of the detection are other critical parameters for point-of-care diagnostic applications.[32]

In this article, we overview the recent progress in single nanoparticle techniques based on electrical, mechanical and optical detection with the primary emphasis on the label-free optical sensing. The techniques are mainly discussed in terms of their transduction mechanisms and how they address the challenges mentioned above.

2 Electrical techniques

The fundamental principle of the electrical detection is based on probing conductance or capacitance change on a local sensing element. One of the approaches is to use conducting or semi-conducting nanowire based field effect transistor devices.[33] In a typical detection scheme, an impedance measurement is performed between source and drain terminals of the nanowire while a solution containing the nanoparticles of interest either flowed through or incubated with the device. As a nanoparticle with different electrical properties than the local environment adsorbs onto the nanowire, it perturbs the local electrical properties of the wire, resulting in a detectable signal on the impedance measurement. In an earlier study, Patolsky *et al.*[34] demonstrated the specific detection of single Influenza-A and paramyxovirus in a buffer solution based on conductance measurements on silicon nanowire arrays functionalized with specific antibodies for each virus type. A difficulty associated with the field effect based techniques is that the detection is sensitive to the ion concentration of the solution. In particular, the detection sensitivity may suffer significantly in high ion concentrations due to charge screening effects limiting the direct use of physiological solutions.[35]

An alternative technique to the nanowire based field effect devices is to probe the impedance change across a nanoscale aperture.[36–39] In contrast to field-effect transistor devices, impedance measurement is performed along a channel and the impedance is perturbed as a nanoparticle with different electrical properties than the solution passes through the nanoscale channel. In a recent study, a high-throughput microfluidic device utilizing a nanoscale aperture is demonstrated for detection and sizing single polystyrene nanoparticles down to 51 nm in diameter and T7 bacteriophage viruses in salt and blood plasma solutions (Fig. 1).[38] Nanoaperture based techniques characteristically offer very rapid and high-throughput detection since no specific/unspecific surface capture of nanoparticles is involved; however, affinity-specific detection is not technically possible

which may hamper the adoption of these techniques in clinical biosensing studies. For example, the size-specific detection of small viruses in blood plasma was shown to be challenging without affinity based capture as the large number of background nanoparticles in blood plasma hinders the detection of virus concentrations comparable to clinically relevant viral loads.[38]

One advantage of the electrical methods is their compatibility with established microelectronic manufacturing technology. The sensing electronics can be easily integrated with microfluidic structures on the same chip providing a robust and cost-effective platform for numerous lab-on-chip applications.

3 Mechanical techniques

The primary component of most single nanoparticle mechanical detectors is a microcantilever of which the adsorbed nanoparticles alter the static or dynamic mechanical response. Among various alternatives, the detectors based on measuring the frequency shift of the oscillating high-Q cantilever have shown promise.[40–48] These devices typically require vacuum conditions to operate in since a high-Q factor cannot be retained in air or liquid solution due to viscosity losses. Therefore, the reported studies in the literature have been limited to end-point detection of nanoparticles.[40,42] Note that, the mechanical response of the cantilevers is sensitive to the exact location of particle binding. Therefore, quantitative mass analysis may become imprecise if the binding site on the cantilever, whose typical size is tens of microns, is not known.

Suspended microchannel resonators (SMRs) are a viable alternative to the conventional cantilever resonators for the applications requiring quantitative and real-time analysis.[45] In SMRs, the solution containing the nanoparticles is transported in microfluidic channels that are fabricated into the cantilever. Therefore, SMRs can be operated under vacuum conditions allowing high-Q resonant measurements in real-time. In a recent study, Lee *et al.* demonstrated single gold nanoparticle detection down to 20 nm in diameter using a SMR based mechanical detector with a 1 kHz detection bandwidth (Fig. 2).[46] They further showed the dynamic control of the flow of the solution to trap single nanoparticles at the tip of the cantilever to improve the sensitivity of the mass estimation. Their results suggest that the detection of individual viruses with a similar mass, such as HIV, could be possible.

The scalable fabrication of the cantilevers on substrates makes these devices useful for applications demanding high-throughput and real-time measurement. However, the requirement of vacuum in the cavity of the cantilever for sensitive detection may hinder their widespread use in point-of-care applications due to the cost and handling issues. A further aspect of the mechanical detection is the actuation mechanisms which are not discussed here. The interested readers are referred to other references.[49]

4 Optical techniques

In 17th century, van Leeuwenhoek developed first powerful microscopes known to detect *animalcules* or microorganisms in a drop of water for the first time.[50] Since then, microscopes have been the essential tools in biology for visual investigation of micron size particles. Fluorescence labeling techniques have been successfully employed to increase both the sensitivity and the resolution of the optical microscope.[51–53] However, the complications associated with a laborious labeling process, high cost and undesired interference of the fluorescence molecules on the characteristics of the target particle have limited their use in nanoparticle detection applications. In the last decade, several advanced microscopic techniques and optical waveguide based devices involving high-Q resonators have been developed in order to detect and characterize single nanoparticles in a label-free

fashion. In addition to the optical techniques above, near-field techniques utilizing a scanning probe to optically characterize the nanoparticles also have been demonstrated.[54,55] However, the near-field techniques are excluded in the discussion here. The interested readers are referred to other references.[31] Recent progress in both microscopic and optical waveguide based label-free methods is discussed below.

4.1 Microscopic techniques

Interferometric microscopy—Microscopic studies of nanoparticles typically involve illuminating the nanoparticles with a coherent or incoherent visible light source and probing the light scattered or absorbed by nanoparticles using free-space optical elements such as objective lenses and array/single-element detectors. For a small spherical nanoparticle, the scattered intensity at a detector (I_{det}) can be given in a simple form:[56]

$$I_{\mathrm{det}} \propto \left|E_{\mathrm{sca}}\right|^2 \propto \sigma_{\mathrm{sca}} \propto \left|\frac{\varepsilon_p - \varepsilon_m}{\varepsilon_p + 2\varepsilon_m}\right|^2 R^6 \quad (1)$$

where E_{sca} and σ_{sca} correspond to scattered field and scattering cross-section, respectively. The scattered intensity at a given wavelength of light depends on the dielectric index of the nanoparticle (ε_{p}) and surrounding medium (ε_{m}) as well as the radius of the nanoparticle (R). The strong dependence of the scattered intensity on the particle size renders the small nanoparticles usually difficult to detect. One approach to overcome this difficulty relies on interferometric detection in which the weak scattered field is mixed with a stronger reference field (E_{ref}). In a typical homodyne interferometric measurement, the detected intensity can be expressed as:[57,58]

$$I_{\mathrm{det}} \propto |E_{\mathrm{ref}} + E_{\mathrm{sca}}|^2 \propto |E_{\mathrm{ref}}|^2 + E_{\mathrm{sca}}|^2 + 2|E_{\mathrm{ref}}||E_{\mathrm{sca}}|\cos\theta_{\mathrm{rs}} \quad (2)$$

where θ_{rs} refers to the phase angle difference between reference and scattered fields. The first term contributes as a constant background intensity, the second term usually vanishes for small nanoparticles because of its R^6 dependence and the third term typically forms the dominant optical response of the nanoparticle with R^3 scaling factor.

Interferometric techniques were initially applied for characterizing single plasmonic metallic nanoparticles.[59,60] At surface plasmon resonance (SPR) wavelength (λ_{SPR}), the scattering cross-section of a metallic nanoparticle is significantly enhanced as the following condition typically holds: $|(\varepsilon_{\mathrm{p}}(\lambda_{\mathrm{SPR}}) - \varepsilon_{\mathrm{m}})/(\varepsilon_{\mathrm{p}}(\lambda_{\mathrm{SPR}}) + 2\varepsilon_{\mathrm{m}})| \gg 1$ in eqn (1). The characteristic spectral dependence of the SPR behavior allows metallic nanoparticles to be distinguished among other nanoparticles and also provides additional information about its local environment and intrinsic physical properties such as shape anisotropy.[60] Interferometric techniques have also been demonstrated for detecting single dielectric nanoparticles including synthetic and natural particles. The optical properties of dielectric nanoparticles differ from the metallic nanoparticles in two important ways. First, dielectric nanoparticles do not exhibit distinct spectral resonances in the visible spectral region and, second, they provide a low index contrast to the background ($|(\varepsilon_{\mathrm{p}} - \varepsilon_{\mathrm{m}})/(\varepsilon_{\mathrm{p}} + 2\varepsilon_{\mathrm{m}})| \ll 1$) which renders the detection difficult compared to similar sized metallic nanoparticles under resonance.

In earlier studies, the interferometric detection was demonstrated for gold nanoparticles fixed on a glass substrate.[60–63] The mixing of scattered light from nanoparticles and reference light from the glass substrate allowed detection of nanospheres down to 5 nm in diameter.[60] Also, higher order laser beams are utilized to differentiate nanospheres and nanorods for which the orientation can also be accurately determined.[62,63] Despite the increased sensitivity, the dimension based analysis of the nanoparticles was limited due to

the double valued optical response curve of the nanoparticles as a function of dimension.[60,62]

In their interferometric reflectance imaging sensor (IRIS), Daaboul *et al.* circumvented the ambiguity in sizing due to non-unique optical response by using a layered reflective substrate.[64] The layered substrate which was composed of a thin oxide spacer layer grown on top of a silicon chip allowed dynamic control over the optical response of the nanoparticles as the illumination wavelength could be chosen in the course of a measurement. Since the optical path provided by the spacer layer was different for distinct wavelengths, the phase relation between the reference and scattered fields (the cosine term in eqn (2)) could be tuned to maximize the signal for different nanoparticle populations of interest. The precise thickness of the layered substrate allowed real-time calibration for measuring the absolute size of the nanoparticles by comparing the signal from the nanoparticle to the background in the vicinity of the nanoparticle. As opposed to earlier studies, the wide-field imaging scheme with a multi-color illumination source based on discrete LED sources allowed them to simultaneously study nanoparticles in a parallel fashion. Based on this design, they demonstrated high-throughput detection and size determination for H1N1 viruses and polystyrene nanoparticles fixed on the substrate (Fig. 3). In a following study, the same group extended their analysis to measure the dimensions of gold nanorods through controlling the polarization of the incident radiation (Fig. 4). This shape sensitive detection scheme was also applied to detect bullet shaped vesicular stomatitis viruses recently.[65] The results obtained in the study show promise for morphology specific virus detection.

Another promising interferometry approach is heterodyne detection. In a typical experimental setting, a known frequency shift is introduced between the reference and the signal arm to selectively determine the contributions from the phase and amplitude of the interferometric term in eqn (2). Hong *et al.* combined a cross-polarization interferometry with heterodyne scheme to detect 5 nm gold nanoparticles immobilized on a glass substrate.[66] Also, Mitra *et al.* demonstrated real-time detection of sub-100 nm polystyrene and as well as HIV, Influenza and Sindbis viruses flowing through a microfluidic channel (Fig. 5).[67] In their differential heterodyne detection scheme, the nanoparticles were classified in size with R^3 scaling of the detector signal amplitude. In a following study, Deutsch *et al.* used a dual-phase interferometry instead of optical heterodyning to decouple the phase and amplitude of the interferometric response thus eliminating active optical components in the setup.[68] The authors utilized a numerical aperture increasing lens in order to achieve higher detection sensitivity compared to air objectives while ensuring a compact and scalable instrument design.

In optical techniques, the detected signal depends on both the geometry and the dielectric constant of the nanoparticles in a given surrounding environment as eqn (1) indicates. Several interferometric techniques have shown that the effects of these two contributions can be independently determined to classify the nanoparticles in terms of material property. For instance, the IRIS technique has been used to distinguish gold and silver nanoparticles in a mixture. The technique was based on adjusting the thickness of the spacer layer between the particle and reflective silicon substrate such that the optical response as a function of defocus is unique for each material type.[69] The maxima and minima observed on the defocus response as shown in Fig. 6a for each particle allowed material specific classification. Fig. 6b shows the distinct image characteristics of the 52 nm Au particles from 72 nm Ag particles at a given defocus plane. Also, Person *et al.* demonstrated the material specific detection of gold and silver nanoparticles flowing through a microfluidic channel.[70] By using a dual-color beam for which the slope of the scattering cross-section is in the opposite sign for 60 nm silver and 80 nm gold nanoparticles, the nanoparticles in a

heterogeneous mixture were classified in terms of their differential optical response. In a similar study, Luo *et al.* used a multi-wavelength differential interference contrast microscope to demonstrate multiplexed detection of gold, silver and polystyrene nanoparticles on a human cancer cell membrane.[71]

The interferometric methods discussed above offer nanoparticle characterization either in space or time domain multiplexing schemes in which the nanoparticles either adsorb onto a surface or pass through the focus of the laser beam, respectively. One advantage of the multiplexing in space domain is the following: numerous individual nanoparticles can be simultaneously investigated with respect to their specific interaction with a functionalized surface site. This capability is indispensable for applications requiring affinity-specific nanoparticle detection in complex solutions including background nanoparticles, such as specific virus detection in a blood sample. Alternatively, time domain multiplexing schemes such as solution based flow-through detectors may be advantageous for the detection applications which do not involve affinity specific interactions. For example, the sample solution can be recycled and preserved for further analysis.

Absorption microscopy—Another sensitive method for detection is to measure the light absorbed by single nanoparticles.[72] If the size of a particle is very small compared to the wavelength of an incident beam, the absorption cross-section of the particle is given by:[56]

$$\sigma_{\mathrm{abs}} \propto Im\left[\frac{\varepsilon_{\mathrm{p}} - \varepsilon_{\mathrm{m}}}{\varepsilon_{\mathrm{p}} + 2\varepsilon_{\mathrm{m}}}\right] R^3 \quad (3)$$

A comparison of eqn (3) to eqn (1) shows that the absorption may significantly dominate over scattering for small nanoparticles with imaginary dielectric functions at a given wavelength. Based on this principle, several sensitive methods have been developed to detect very small metallic nanoparticles down to a few nanometres in size.[72–79] In an earlier study, Arbouet *et al.* used a spatial modulation technique to determine the absolute absorption cross-section of single gold nanoparticles as small as 5 nm.[77] In their experiment, a focused laser beam transmitted through a nanoparticle is detected in a lock-in scheme while the position of the nanoparticle in the focus is modulated at a constant frequency on the transverse plane. In a following study, Muskens *et al.* adapted the spatial modulation technique for performing polarization sensitive spectroscopy in order to determine the size and shape of gold and silver nanoparticles.[78] Despite the complicated optical setup, the spatial modulation technique can be useful for the applications requiring characterization of small metallic nanoparticles in terms of size and shape. In addition to the direct way of measurement, the absorption cross-section can also be investigated indirectly by monitoring the photo-thermal effects created by the absorbing nanoparticle. Berciaud *et al.* developed a sensitive photo-thermal heterodyne imaging method for detecting individual gold nanoparticles down to 1.4 nm in size as well as semiconducting nanocrystals.[79] In this method, a probe beam interacts with the time modulated variations of the refractive index in the vicinity of the absorbing nanoparticle generated by an additional heating beam and gives rise to a scattered field containing sidebands with a frequency of the modulation. Then the beat-note created by the interference of the scattered field by the perturbation and a reference probe beam is detected in a lock-in scheme. One of the advantages of this technique is that a background-free image can be obtained since any non-absorbing background scatterers do not produce a detectable signal. However, the thermal effect generated by the heating beam might pose challenges for applications requiring thermal stability. This technique has been adapted for various biological studies including estimation of protein stoichiometry of a single virus-like particle and measurement of local cytosol viscosity in live cells.[80,81]

Surface plasmon resonance microscopy—A promising method to detect nanoparticles is Surface Plasmon Resonance Microscopy (SPRM). In most SPRM techniques, a collimated and polarized light beam impinges upon a glass substrate coated with a thin layer of metal at a specific configuration so that surface plasmon waves are excited on the surface of the thin metal layer; and the specular reflection from the substrate is imaged onto an array detector thus forming a spatial image of the illuminated area. The contrast mechanism in a typical SPRM is based on the local refractive index change in the vicinity of the surface of the metallic layer. Since the resonant excitation of the surface plasmon waves is sensitive to the local refractive index in the vicinity of the metal layer, any perturbation in the local index such as binding of a nanoparticle on the metal surface provides a discernible signature on the spatial image obtained on the array detector. Although numerous SPRM techniques have been extensively used to probe bimolecular interactions of proteins, nucleic acids, allergens, biomarkers, *etc*., only a few studies have reported the detection of single nanoparticles. In a recent study, Wang *et al*. studied detection of single silica nanoparticles down to 98 nm in diameter as well as dynamic interaction of single H1N1 viruses in a buffer solution with different functionalized surfaces (Fig. 7).[82] A promising approach to increase the sensitivity of the SPRM techniques is replacing the uniform thin layer of metal with nanoscale antennas which localize the surface plasmon waves and thus leading further enhanced interaction between nanoparticle and light in the hot spots. In a recent study, Zhang *et al*. utilized a plasmonic dipole antenna in order to trap and sense single gold nanoparticles as small as 10 nm in diameter.[83] The resonance shift in the scattering spectrum of the dipole antenna was monitored in real time as the small nanoparticles were trapped in the gap due to strongly localized fields. In particular, this technique shows promise for detection of single nanoparticles through highly specific chemical fingerprint probing *via* Raman spectroscopy.[84,85] The throughput of this technique is significantly hampered due to the technically demanding fabrication of the nanoantennas with current manufacturing methods. However, emerging fabrication methods may help to improve the throughput capacity of this technique in the near future.[86,87]

4.2. Optical waveguide device based techniques

Optical waveguides are an alternative way of guiding the light beam to the free-space optical components such as lenses and mirrors. A simple waveguide is composed of a two-dimensional structure with a high-index core in which the optical wave is largely confined and a low index cladding through which the evanescent tail of the wave extends typically less than a wavelength of the light beam. In a typical waveguide based photonic device, a nanoparticle in close proximity to waveguide interacts with the evanescent tail of the optical wave and consequently perturbs the wave distribution in the vicinity of the waveguide. This perturbation has been probed in many different device geometries and transduction configurations in order to detect the presence of a nanoparticle in the surrounding of the waveguide. One approach to sense the perturbation is using an interferometric detection scheme measuring the optical path difference between a signal arm on which the nanoparticle binds and a reference arm that is protected from nanoparticles. Then the optical path difference between two arms is determined through either coupling the waves in both waveguide arms on chip as in Mach–Zehnder inter-ferometry or performing free-space interferometry as in Young and Hartman interferometries.[88,89] In a simple model, the optical path difference in terms of phase difference ($\Delta\varphi$):

$$\Delta\phi \propto l\lambda^2\Delta n \quad (4)$$

where l, λ and Δ_n are the effective interaction length of the signal waveguide arm, wavelength of light and relative index change in the surrounding of the waveguide, respectively. For a given Δ_n, the sensitivity of an interferometric device can be increased by

using longer wavelengths; however, in a typical application setting, the waveguide is operated in a buffer solution which typically absorbs the longer wavelengths, thus decreasing the light–nanoparticle interaction due to the excess loss. Alternatively, the effective interaction length (l) term can be increased in order to realize stronger light–nanoparticle interaction. However, the effective interaction length is characteristically determined by the nanoparticle itself in the single particle limit.

A promising way to increase the effective interaction length is using resonant microcavity structures in which the light samples a nanoparticle many times before being detected.[90–96] In a typical resonant cavity based device, the light coupled to the cavity circulates within the structure forming whispering gallery modes at specific resonant wavelengths before it couples back to a bus waveguide on which the detection is performed. Any interaction of nanoparticles with the evanescent tail of the optical wave on the resonator perturbs the resonance behaviour of WGMs in the cavity. A critical parameter determining the sensitivity of single nanoparticle detection is the quality factor (Q) of the resonant cavity. The value of Q is proportional to the average time a photon circulates in a WGM, in turn controlling the line width of the resonance ($\delta\lambda_r = \lambda_r/Q$). Higher Q values yield narrower spectral resonance widths resulting in more sensitive measurement for resonant cavity photonic devices. Earlier studies in this field focused on determining the real-time resonant frequency jumps owing to adsorbing nanoparticle on the microcavity surface. The resonant wavelength shift ($\Delta\lambda_r/\lambda_r$) can be correlated to the radius of a nanoparticle ($r_p \ll \lambda_r$) that adsorbs onto the equatorial line of the microsphere resonator with a radius R:[97]

$$\left(\frac{\Delta\lambda_r}{\lambda_r}\right) \propto \frac{r^3}{R^{5/2}\lambda_r^{1/2}} \quad (5)$$

The equation above suggests that the sensitivity of the detection and sizing can be increased through shrinking the size of the microcavity. However, the smaller microcavities also lead to reduction in Q due to increased radiation leakage. Vollmer *et al.* demonstrated detection and sizing of individual Influenza viruses ($r \approx 50$ nm) using an optimal size microsphere resonator situated in a fluidic cell filled with a buffer solution of Influenza-A virus.[98] Note that nanoparticle sizing based on the resonant frequency shift mechanism can be sensitive to environmental noise including the temperature, laser beam intensity and laser frequency fluctuations which may cause undesired drifts and jumps in the resonant frequency. In a recent study, Lu *et al.* incorporated a reference interferometer into a high-Q microcavity to increase the accuracy and sensitivity of the nanoparticle detection (Fig. 8).[99] In this configuration, the reference interferometry was used to measure the laser frequency accurately in parallel to the nanoparticle detection performed on a microtoroid resonator. Therefore, the error originating from the frequency jitter and laser scan-voltage measurement was reduced. It was demonstrated that Influenza A viruses can be detected with a signal to noise ratio of 38 : 1 which is about an order of magnitude improvement over previous studies.

A critical drawback of the methods based on frequency shift mechanism is that the signal amplitude is sensitive to the binding position of the nanoparticle on the resonator. A nanoparticle yields a large frequency shift if it binds to the region where the interaction between the evanescent tail of the WGM and the nanoparticle is maximum and the signal generated with the same particle will decrease if the particle is adsorbed away from this region. An alternative method addressing this issue is to monitor the mode splitting of the WGM.[100] Mode splitting of a WGM occurs when the scattering from a nanoparticle lifts the degeneracy of clockwise and counter-clockwise propagating modes of the WGM in a resonator. Resulting splitting and line width of the doublets can be used to determine the nanoparticle size:[101]

$$r^3 \propto \lambda_r^2 \left(\frac{\Gamma_r}{g} \right) \quad (6)$$

where Γ_r and g denote the line width broadening and coupling strength between two propagating modes, respectively, and these quantities can be calculated from the measured spectra by fitting a double Lorentzian function to the resonance line. The term $\Gamma(\Gamma_r/g)$ in the equation above is independent of the binding position of the nanoparticle on the surface of the resonator; therefore, the size estimation can be performed more accurately compared to the frequency shift based methods discussed above. Using this method, Zhu *et al.* demonstrated accurate sizing of individual PS particles down to 60 nm in diameter under ambient conditions without any assumption on the location of particle binding (Fig. 9).[101] Note that the accuracy of the fitting of Γ_r and g parameters depends on the line width of the resonance line which is correlated to Q of the microcavity. Sufficiently high Q is necessary to resolve the doublet originating from the nanoparticle detection. For example, adsorbed single Influenza A virus results in a splitting on the order of 30 MHz and a Q factor of 107 is required to directly detect the binding of the virus.[100] Although this value of Q is typically within reach under ambient laboratory conditions, it is challenging to achieve this level of Q in practical settings such as nanoparticles dispersed in buffer solution. Recently an interferometric detection scheme was suggested for increasing the sensitivity of the mode-splitting measurements; thus, it might allow size classification of single virus particles in the near future.[102]

Resonant microcavity based detection is a relatively new but rapidly flourishing subfield of optical techniques for single nanoparticle detection. The recent experimental studies in the literature have been primarily focused on improving the detection limit and sizing sensitivity. Despite the significant advancement on these metrics as discussed above, less attention has been paid to other metrics such as shape recognition and material/affinity specific detection of single nanoparticles. Also a critical setback for the practical implementation of these devices is the limited throughput capacity. One of the reasons is that the detection scheme of the resonant microcavities requires perturbation of the WGM resonating in the structure by the nanoparticle. Each interacting nanoparticle therefore changes the characteristics of the WGM such as introducing damping channels, reducing the Q factor, *etc.* The number of individual nanoparticles detected by a microcavity resonator must be limited in order to preserve the original sensitivity of the microcavity device. This requirement can be satisfied by increasing the number of resonators in a multiplexed fashion on a detection device. However, it is demanding to fabricate many resonant microcavities with identical optical specifications such as resonant frequencies and quality factors using the current fabrication methods. Provided that these challenges are addressed, optical microcavity based devices will find a wide range of applications for single nanoparticle detection.

5 Conclusions

In this article, we discussed a number of recent techniques for label-free detection and characterization of individual nanoparticles. We believe that individual nanoparticle characterization will have a major impact on the advancement of many fields in biosciences and biotechnology. Individual nanoparticle characterization will allow the study of how physical properties including size and shape of these nanoparticles will affect their functionality. For example, nanoparticles being designed for drug delivery could be further optimized by studying how morphology affects binding affinity and specific targeting. This new information will allow a more systematic approach in the design of these nanoparticles.

Single nanoparticle techniques can also serve as very sensitive biosensors for the detection of natural nanoparticles such as viruses that have been a serious threat to human health. Many of the techniques discussed in this review have shown virus detection capability in buffer solutions but have not demonstrated highly sensitive detection in complex solutions like sera or environmental samples. The limitations of these sensors are sensor size and diffusion, the latter due to the 2D structure of the detection surface. We believe that if these limitations are addressed through the integration of better sample preparation and delivery methods using microfluidics and lab-on-chip techniques, the performance of these sensors will improve significantly and they will find practical use in real-world sensing applications.

Acknowledgments

This work was supported in part by US Army Research Laboratories (ARL) grant W911NF-06-2-0040.

Biographies

Abdulkadir Yurt received his BS degree in Microelectronics from Sabanci University, Istanbul, in 2008. He is currently pursuing a PhD degree in Materials Science and Engineering at Boston University. His research interests include label-free optical single nanoparticle detection and optical microscopy for fault isolation and failure analysis of semiconductor devices.

George G. Daaboul received his BS degree in Biomedical Engineering from Boston University in 2009. He is currently pursuing a PhD in Biomedical Engineering at Boston University. His research interests include label-free optical biosensors for pathogen detection for clinical and biodefense applications.

John H: Connor received his BA degree in Chemistry from Swarthmore College, Swarthmore, PA, in 1994, and a PhD in Pharmacology from Duke University, in 1999. He was a Postdoctoral Fellow at Wake Forest University. In 2006, he joined the faculty of Boston University School of Medicine, Boston, MA, where he is currently an Assistant Professor of Microbiology. His research interests include understanding molecular mechanisms of viral pathogenesis, transcriptomics of the virus-host interaction, and the development of new virus detection technologies.

Bennett B: Goldberg received his PhD degree in Physics from Brown University in 1987. Following a Bantrell Postdoctoral appointment at the Massachusetts Institute of Technology and the Francis Bitter National Magnet Lab, he joined the physics faculty at Boston University in 1989. Currently he is Professor of Physics, with joint appointments as Professor of Biomedical Engineering and Professor of Electrical and Computer Engineering. His research interests include spectroscopy of graphene, nanotube and quantum dots; tip-enhanced near-field spectroscopy of plasmonic structures; and subsurface solid immersion microscopy. His research extends to resonant biosensors for cancer and infectious disease biomarker discovery. He is also the founder and director of the Center for Nanoscience and Nanobiotechnology at Boston University.

M: Selim Ünlü completed his PhD degree in Electrical Engineering at the University of Illinois, Urbana-Champaign, and joined the Department of Electrical and Computer Engineering at Boston University in 1992. He is currently a Professor of Electrical and Computer Engineering, Biomedical Engineering, Physics, and Graduate Medical Sciences. He is also serving as the Associate Dean for research and graduate programs in engineering, as well as the Associate Director of the Center for Nanoscience and Nanobiotechnology. His current research interests include nanophotonics and bio-photonics, high-resolution microscopy and spectroscopy of semiconductor devices and biological materials, and biological sensing and imaging. He is a recipient of the Science Award by the Turkish Scientific Foundation.

References

1. Mazzola L. Nat. Biotechnol. 2003; 21:1137–1143. [PubMed: 14520392]
2. Whitesides GM. Nat. Biotechnol. 2003; 21:1161–1165. [PubMed: 14520400]
3. Sperling RA, Gil PR, Zhang F, Zanella M, Parak WJ. Chem. Soc. Rev. 2008; 37:1896–1908. [PubMed: 18762838]
4. De M, Ghosh PS, Rotello VM. Adv. Mater. 2008; 20:4225– 4241.
5. Salata OV. J. Nanobiotechnol. 2004; 2:3.
6. Cognet L, Tardin C, Boyer D, Choquet D, Tamarat P, Lounis B. Proc. Natl. Acad. Sci. U. S. A. 2003; 100:11350–11355. [PubMed: 13679586]
7. Bhirde A, Xie J, Swierczewska M, Chen X. Nanoscale. 2011; 3:142. [PubMed: 20938522]
8. Anker JN, Hall WP, Lyandres O, Shah NC, Zhao J, Van Duyne RP. Nat. Mater. 2008; 7:442–453. [PubMed: 18497851]
9. Haun JB, Yoon TJ, Lee H, Weissleder R. Wiley Interdiscip. Rev.: Nanomed. Nanobiotechnol. 2010; 2:291–304. [PubMed: 20336708]
10. Jain RK, Stylianopoulos T. Nat. Rev. Clin. Oncol. 2010; 7:653–664. [PubMed: 20838415]
11. Peer D, Karp JM, Hong S, Farokhzad OC, Margalit R, Langer R. Nat. Nanotechnol. 2007; 2:751–760. [PubMed: 18654426]

12. Brigger I, Dubernet C, Couvreur P. Adv. Drug Delivery Rev. 2002; 54:631–651.
13. Maynard AD, et al. Nature. 2006; 444:267–269. [PubMed: 17108940]
14. Nel A, Xia T, Madler L, Li N. Science. 2006; 311:622. [PubMed: 16456071]
15. Damoiseaux R, et al. Nanoscale. 2011; 3:1345. [PubMed: 21301704]
16. Somers CM, McCarry BE, Malek F, Quinn JS. Science. 2004; 304:1008. [PubMed: 15143280]
17. Lynch I, Salvati A, Dawson KA. Nat. Nanotechnol. 2009; 4:546–547. [PubMed: 19734922]
18. Martin L, Johannes S, Giuliano E. Proc.Natl.Acad. Sci.U. S.A. 2008; 105:14265–14270. [PubMed: 18809927]
19. Yan L, Zhao F, Li S, Hu Z, Zhao Y. Nanoscale. 2011; 3:362– 382. [PubMed: 21157592]
20. WHO. World Health Statistics. 2010. p. 2010
21. McLaughlin-Drubin ME, Munger K. Biochim. Biophys. Acta, Mol. Basis Dis. 2008; 1782:127–150.
22. Hausen HZ. Science. 1991; 254:1167–1173. [PubMed: 1659743]
23. Seiki M, Hattori S, Yoshid M. Proc. Natl. Acad. Sci. U. S. A. 1982; 79:6899–6902. [PubMed: 6294664]
24. Pulitzer MP, Amin BD, Busam KJ. Adv. Anat. Pathol. 2009; 16:135–144. [PubMed: 19395876]
25. Hu J, Ludgate L. Cancer Treat. Res. 133:241–252. [PubMed: 17672044]
26. Potter CW, Appl J. Microbiol. 2001; 91:572–579.
27. Bray M. Antiviral Res. 2003; 57:53–60. [PubMed: 12615303]
28. Krug RM. Antiviral Res. 2003; 57:147–150. [PubMed: 12615310]
29. van Dijk MA, Tchebotareva AL, Orrit M, Lippitz M, Berciaud S, Lasne D, Cognet L, Lounis B. Phys. Chem. Chem. Phys. 2006; 8:3486–3495. [PubMed: 16871337]
30. Hunt HK, Armani AM. Nanoscale. 2010; 2:1544–1559. [PubMed: 20820687]
31. Biswas A, Wang T, Biris AS. Nanoscale. 2010; 2:1560–1572. [PubMed: 20661516]
32. Yager P, Domingo GJ, Gerdes J. Annu. Rev. Biomed. Eng. 2008; 10:107–144. [PubMed: 18358075]
33. Lee D, Chander Y, Goyal SM, Cui T. Biosens. Bioelectron. 2011; 26:3482–3487. [PubMed: 21354779]
34. Patolsky F, Zheng G, Hayden O, Lakadamyali M, Zhuang X, Lieber CM. Proc. Natl. Acad. Sci. U. S. A. 2004; 101:14017– 14022. [PubMed: 15365183]
35. Stern E, Wagner R, Sigworth FJ, Breaker R, Fahmy TM, Reed MA. Nano Lett. 2007; 7:3405–3409. [PubMed: 17914853]
36. Uram JD, Ke K, Hunt AJ, Mayer M. Small. 2006; 2:967– 972. [PubMed: 17193151]
37. Sridhar M, Xu D, Kang Y, Hmelo AB, Feldman LC, Li D, Li D. J. Appl. Phys. 2008; 103:104701. [PubMed: 19479001]
38. Fraikin J, Teesalu T, McKenney CM, Ruoslahti E, Cleland AN. Nat. Nanotechnol. 2011; 6:308–313. [PubMed: 21378975]
39. Nguyen BTT, Koh G, Lim HS, Chua AJS, Ng MML, Toh C. Anal. Chem. 2009; 81:7226–7234. [PubMed: 19663392]
40. Hwang KS, Lee S, Kim SK, Lee JH, Kim TS. Annu. Rev. Anal. Chem. 2009; 2:77–98.
41. Godin M, Bryan AK, Burg TP, Babcock K, Manalis SR. Appl. Phys. Lett. 2007; 91:123121.
42. Ilic B, Yang Y, Craighead HG. Appl. Phys. Lett. 2004; 85:2604.
43. Gupta A, Akin D, Bashir R. Appl. Phys. Lett. 2004; 84:1976.
44. Johnson L, Gupta AK, Ghafoor A, Akin D, Bashir R. Sens. Actuators, B. 2006; 115:189–197.
45. Burg TP, Godin M, Knudsen SM, Shen W, Carlson G, Foster JS, Babcock K, Manalis SR. Nature. 2007; 446:1066–1069. [PubMed: 17460669]
46. Lee J, Shen W, Payer K, Burg TP, Manalis SR. Nano Lett. 2010; 10:2537–2542. [PubMed: 20527897]
47. Arlett JL, Roukes ML. J. Appl. Phys. 2010; 108:084701.
48. Naik AK, Hanay MS, Hiebert WK, Feng XL, Roukes ML. Nat. Nanotechnol. 2009; 4:445–450. [PubMed: 19581898]

49. Arlett JL, Myers EB, Roukes ML. Nat. Nanotechnol. 2011; 6:203–215. [PubMed: 21441911]
50. Ford BJ. Trans. Am. Microsc. Soc. 1982; 101:1–9. [PubMed: 7043861]
51. Lichtman JW, Conchello J. Nat. Methods. 2005; 2:910–919. [PubMed: 16299476]
52. Hell SW. Nat. Biotechnol. 2003; 21:1347–1355. [PubMed: 14595362]
53. Rust MJ, Bates M, Zhuang X. Nat. Methods. 2006; 3:793– 796. [PubMed: 16896339]
54. Cvitkovic A, Ocelic N, Hillenbrand R. Nano Lett. 2007; 7:3177–3181. [PubMed: 17880256]
55. Brehm M, Taubner T, Hillenbrand R, Keilmann F. Nano Lett. 2006; 6:1307–1310. [PubMed: 16834401]
56. van de Hulst, HC. Light Scattering by Small Particles. Dover Publications; 1981.
57. Plakhotnik T, Palm V. Phys. Rev. Lett. 2001; 87:183602.
58. Ignatovich FV, Novotny L. Phys. Rev. Lett. 2006; 96:013901. [PubMed: 16486453]
59. Boyer D, Tamarat P, Maali A, Lounis B, Orrit M. Science. 2002; 297:1160. [PubMed: 12183624]
60. Lindfors K, Kalkbrenner T, Stoller P, Sandoghdar V. Phys. Rev. Lett. 2004; 93:037401. [PubMed: 15323866]
61. Jacobsen V, Stoller P, Brunner C, Vogel V, Sandoghdar V. Opt. Express. 2006; 14:405–414. [PubMed: 19503354]
62. Zuchner T, Failla AV, Steiner M, Meixner AJ. Opt. Express. 2008; 16:14635–14644. [PubMed: 18795000]
63. Failla AV, Qian H, Qian H, Hartschuh A, Meixner AJ. Nano Lett. 2006; 6:1374–1381. [PubMed: 16834414]
64. Daaboul GG, Yurt A, Zhang X, Hwang GM, Goldberg BB, Ünlü MS. Nano Lett. 2010; 10:4727–4731. [PubMed: 20964282]
65. Daaboul GG, Lopez CA, Yurt A, Goldberg BB, Connor JH, Ünlü MS. IEEE J. Sel. Top. Quantum Electron. in press.
66. Hong X, van Dijk EMPH, Hall SR, Götte JB, van Hulst NF, Gersen H. Nano Lett. 2011; 11:541–547. [PubMed: 21204579]
67. Mitra A, Deutsch B, Ignatovich F, Dykes C, Novotny L. ACS Nano. 2010; 4:1305–1312. [PubMed: 20148575]
68. Deutsch B, Beams R, Novotny L. Appl. Opt. 2010; 49:4921– 4925. [PubMed: 20830181]
69. Yurt A, Daaboul GG, Goldberg BB, Ünlü MS. unpublished work.
70. Person S, Deutsch B, Mitra A, Novotny L. Nano Lett. 2011; 11:257–261. [PubMed: 21142033]
71. Luo Y, Sun W, Gu Y, Wang GF, Fang N. Anal. Chem. 2010; 82:6675–6679. [PubMed: 20614872]
72. Gaiduk A, Yorulmaz M, Ruijgrok PV, Orrit M. Science. 2010; 330:353–356. [PubMed: 20947760]
73. Octeau V, Cognet L, Duchesne L, Lasne D, Schaeffer N, Fernig DG, Lounis B. ACS Nano. 2009; 3:345–350. [PubMed: 19236070]
74. van Dijk MA, Lippitz M, Stolwijk D, Orrit M. Opt. Express. 2007; 15:2273–2287. [PubMed: 19532462]
75. Muskens OL, Billaud P, Broyer M, Del Fatti N, Vallée F. Phys. Rev. B: Condens. Matter Mater. Phys. 2008; 78:205410.
76. Roland T, Berguiga L, Elezgaray J, Argoul F. Phys. Rev. B: Condens. Matter Mater. Phys. 2010; 81:235419.
77. Arbouet A, Christofilos D, Del Fatti N, Vallée F, Huntzinger JR, Arnaud L, Billaud P, Broyer M. Phys. Rev. Lett. 2004; 93:127401. [PubMed: 15447305]
78. Muskens OL, Del Fatti N, Vallée F, Huntzinger JR, Billaud P, Broyer M. Appl. Phys. Lett. 2006; 88:063109.
79. Berciaud S, Cognet L, Blab GA, Lounis B. Phys. Rev. Lett. 2004; 93:257402. [PubMed: 15697940]
80. Vieweger M, Goicochea N, Koh ES, Dragnea B. ACS Nano. 2011; 5:7324–7333. [PubMed: 21854038]
81. Leduc C, Jung J, Carney RR, Stellacci F, Lounis B. ACS Nano. 2011; 5:2587–2592. [PubMed: 21388224]

82. Wang S, Shan X, Patel U, Huang X, Lu J, Li J, Tao N. Proc. Natl. Acad. Sci. U. S. A. 2010; 107:16028–16032. [PubMed: 20798340]
83. Zhang W, Huang L, Santschi C, Martin OJF. Nano Lett. 2010; 10:1006–1011. [PubMed: 20151698]
84. Nie S, Emory SR. Science. 1997; 275:1102–1106. [PubMed: 9027306]
85. Shanmukh S, Jones L, Driskell J, Zhao Y, Dluhy R, Tripp RA. Nano Lett. 2006; 6:2630–2636. [PubMed: 17090104]
86. Vazquez-Mena O, Sannomiya T, Villanueva LG, Voros J, Brugger J. ACS Nano. 2011; 5:844–853. [PubMed: 21192666]
87. Aksu S, Yanik AA, Adato R, Artar A, Huang M, Altug H. Nano Lett. 2010; 10:2511–2518. [PubMed: 20560536]
88. Ymeti A, Greve J, Lambeck PV, Wink T, van Hovell S, Beumer TAM, Wijn RR, Heideman R, Subramaniam V, Kanger JS. Nano Lett. 2007; 7:394–397. [PubMed: 17298006]
89. Schneider BH, Edwards JG, Hartman NF. Clin. Chem. 1997; 43:1757–1763. [PubMed: 9299972]
90. Armani AM, Kulkarni RP, Fraser SE, Flagan RC, Vahala KJ. Science. 2007; 317:783–787. [PubMed: 17615303]
91. Wang S, Broderick K, Smith H, Yi Y. Appl. Phys. Lett. 2010; 97:051102.
92. Lee M, Fauchet PM. Opt. Lett. 2007; 32:3284–3286. [PubMed: 18026281]
93. Li H, Guo Y, Sun Y, Reddy K, Fan X. Opt. Express. 2010; 18:25081–25088. [PubMed: 21164854]
94. Pineda MF, Chan LL, Kuhlenschmidt T, Choi CJ, Kuhlenschmidt M, Cunningham BT. IEEE Sens. J. 2009; 9:470–477.
95. Lin S, Schonbrun E, Crozier K. Nano Lett. 2010; 10:2408– 2411. [PubMed: 20545333]
96. He L, Özdemir ŞK, Zhu J, Kim W, Yang L. Nat. Nanotechnol. 2011; 6:428–432. [PubMed: 21706025]
97. Vollmer F, Arnold S. Nat. Methods. 2008; 5:591–596. [PubMed: 18587317]
98. Vollmer F, Arnold S, Keng D. Proc. Natl. Acad. Sci. U. S. A. 2008; 105:20701–20704. [PubMed: 19075225]
99. Lu T, Lee H, Chen T, Herchak S, Kim J, Fraser SE, Flagan RC, Vahala K. Proc. Natl. Acad. Sci. U. S. A. 2011; 108:5976–5979. [PubMed: 21444782]
100. Chantada L, Nikolaev NI, Ivanov AL, Borri P, Langbein W. J. Opt. Soc. Am. B. 2008; 25:1312–1321.
101. Zhu J, Özdemir ŞK, Xiao Y, Li L, He L, Chen D, Yang L. Nat. Photonics. 2009; 4:46–49.
102. Knittel J, McRae TG, Lee KH, Bowen WP. Appl. Phys. Lett. 2010; 97:123704.

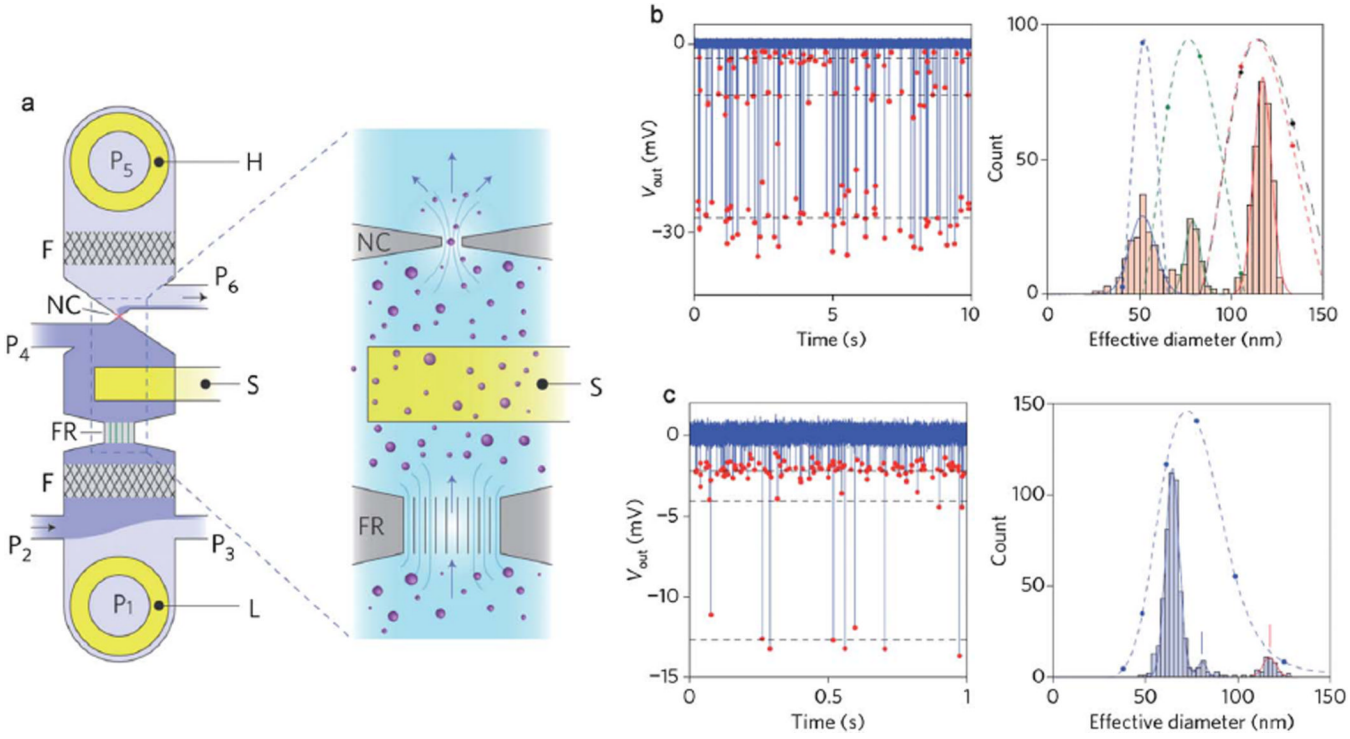

Fig. 1.

Nanoconstriction based detection of single nanoparticles and viruses. (a) The schematic demonstrating the device layout: external voltage bias electrodes (H and L) and sensing electrode (S); embedded filters (F); fluid resistor (FR); nanoconstriction (NC); pressure regulated fluidic ports (P1–P6). Nanoparticles in saline suspension flow in the direction of the arrows, and changes in the electrical potential of the fluid adjacent to the nanoconstriction are detected by the sensing electrode S. (b) Analysis of a nanoparticle solution mixture containing 51 nm, 75 nm and 117 nm polystyrene nanoparticles. Left panel shows the output voltage read as a function of time as the nanoparticles pass through the nanoconstriction. Right panel shows the histogram of effective diameter of the nanoparticles detected. (c) Analysis of T7 bacteriophage viruses with an admixture of 117 nm calibration nanoparticles. Left and right panels show the time-trace plot of output voltage and the histogram of effective diameter of detected particles. The dashed lines correspond to DLS measurement of the mixtures. Adapted from ref. 38. ©2011 Macmillan Publishers Ltd: Nature Nanotechnology.

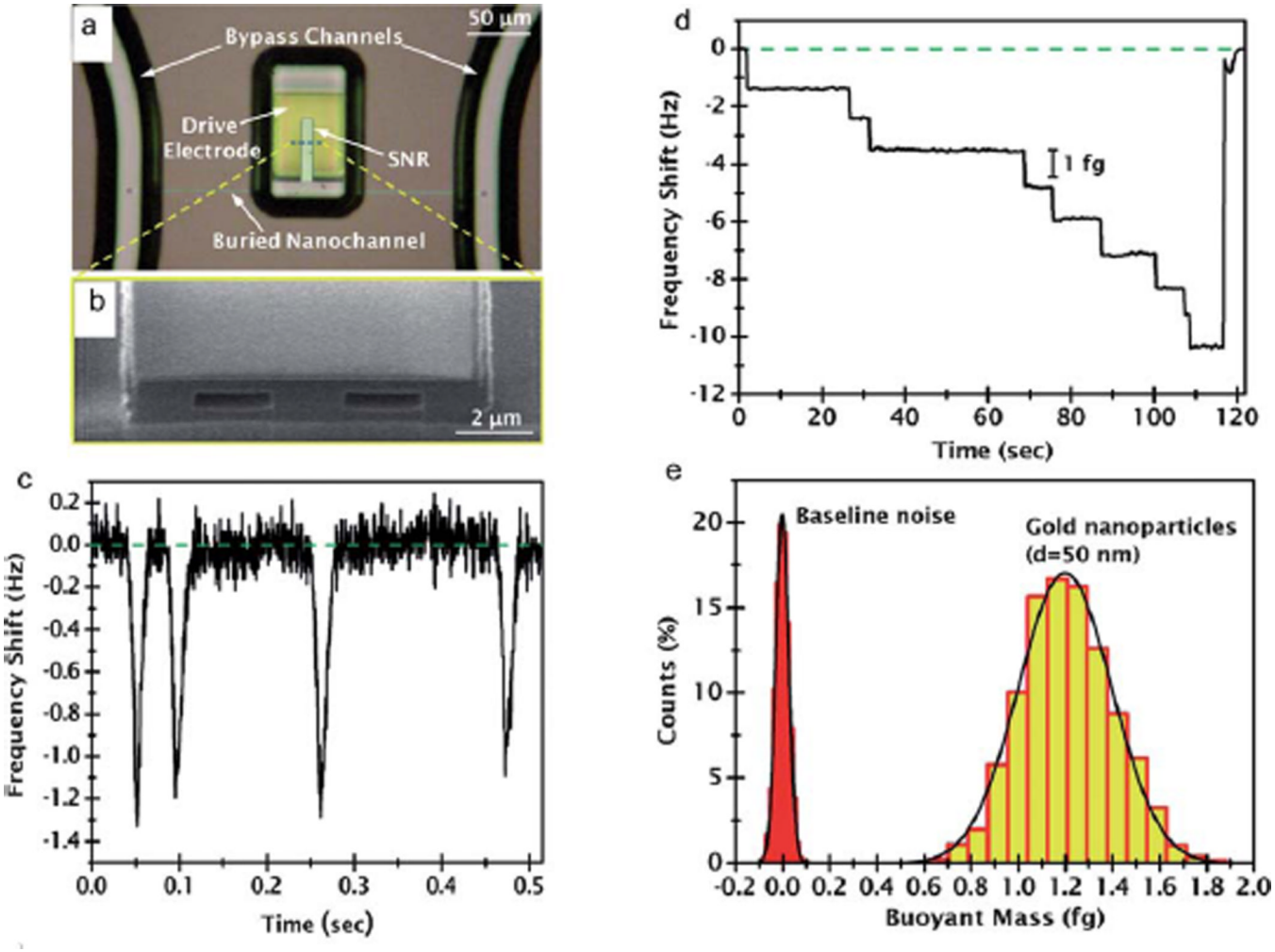

Fig. 2.

SMR based detection of gold nanoparticles. (a) Optical micrograph of the fabricated structure. (b) SEM image of the cutaway view of the structure showing the buried nanofluidic channel. (c) Resonance frequency shift of the cantilever when 50 nm diameter gold nanoparticles flow through the resonator. (d) Resonance frequency shift steps as individual gold nanoparticles are trapped at the tip of the cantilever. (e) The histogram showing the measured mass distribution of 50 nm gold nanoparticles in flow-through mode. The baseline noise is also demonstrated for comparison. Adapted from ref. 46. © 2011 American Chemical Society.

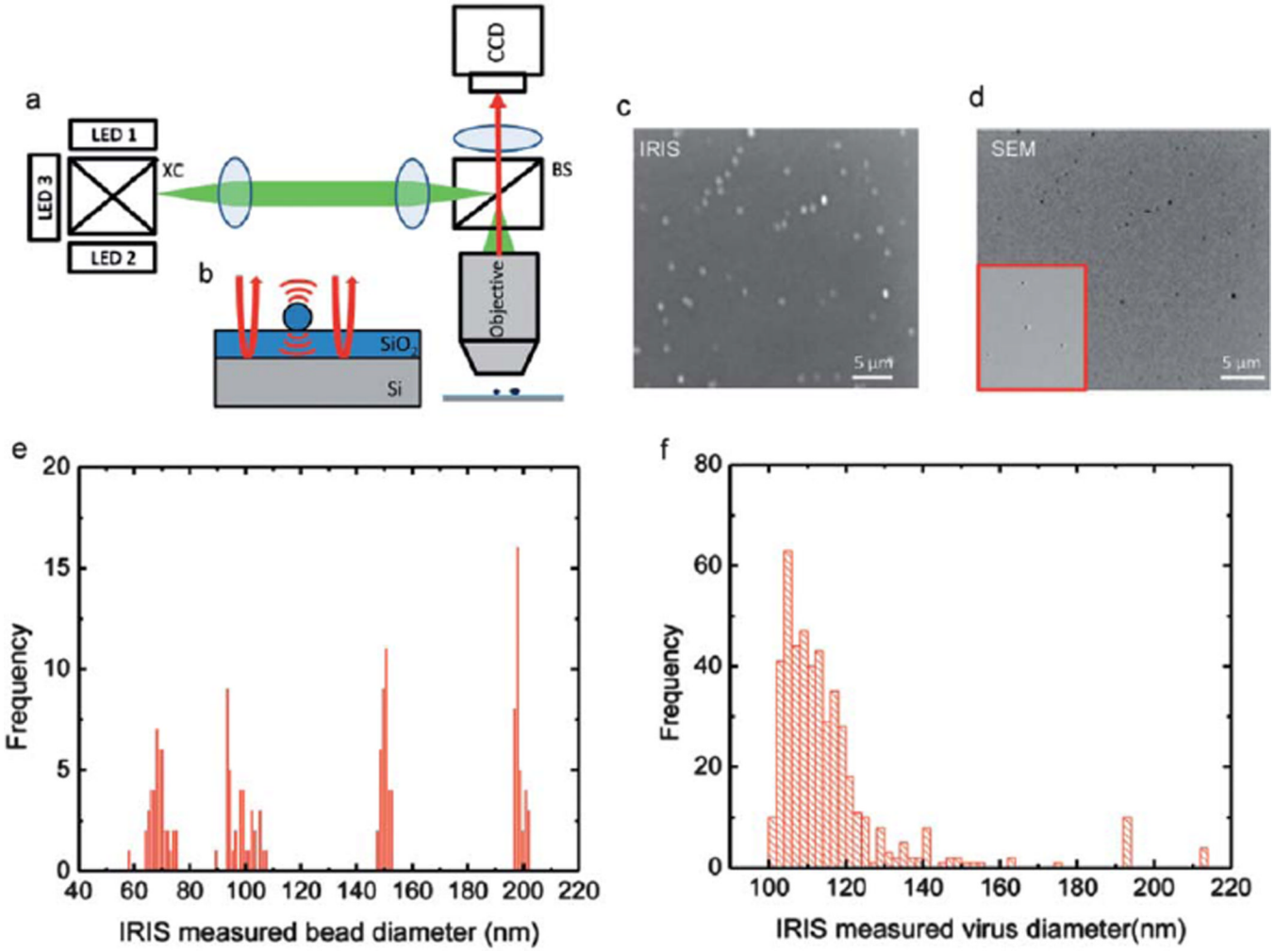

Fig. 3.

Interferometric Reflectance Imaging Sensor (IRIS). (a) Schematic of the optical setup. The setup consists of a multi-wavelength LED light source that is set up in Kohler illumination with a 50 × 0.8NA objective. The sample is imaged at a single wavelength using a CCD camera. (b) The close-up schematic of the object space where the scattered and reflected fields are shown. (c) IRIS image of immobilized virus on the surface with the same field of view as the SEM image. (d) SEM image of the immobilized virus on the surface. (e) Size distribution of single particles on different chips. (f) Measured size distribution of the immobilized virus using IRIS. Adapted from ref. 64. © 2010 American Chemical Society.

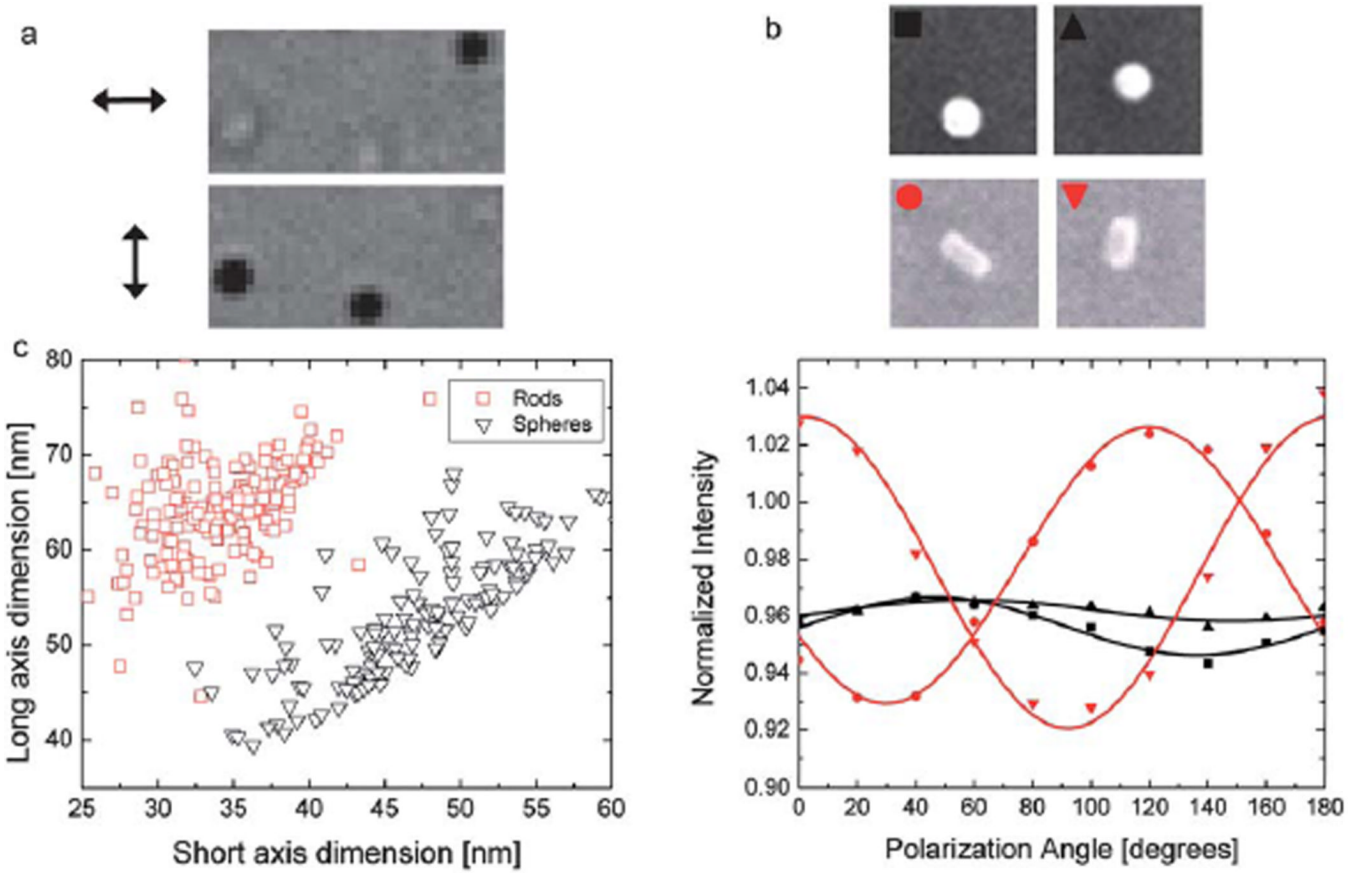

Fig. 4.

Morphology measurement of nanoparticles using IRIS. (a) Optical image of three gold nanorods (nominally 30 nm by 70 nm) for two orthogonal polarization of incident light. (Arrows show the polarization of the incident light.) (b) Comparison of IRIS and SEM measurements for two gold nanospheres (nominally, d = 46 nm) and two nanorods (nominally, 30 nm by 70 nm). The data points and the solid curves show the experimental values and numerical fit to data points for dimension analysis, respectively. (c) High-throughput analysis of nanorod and nanosphere populations on a scatter chart.

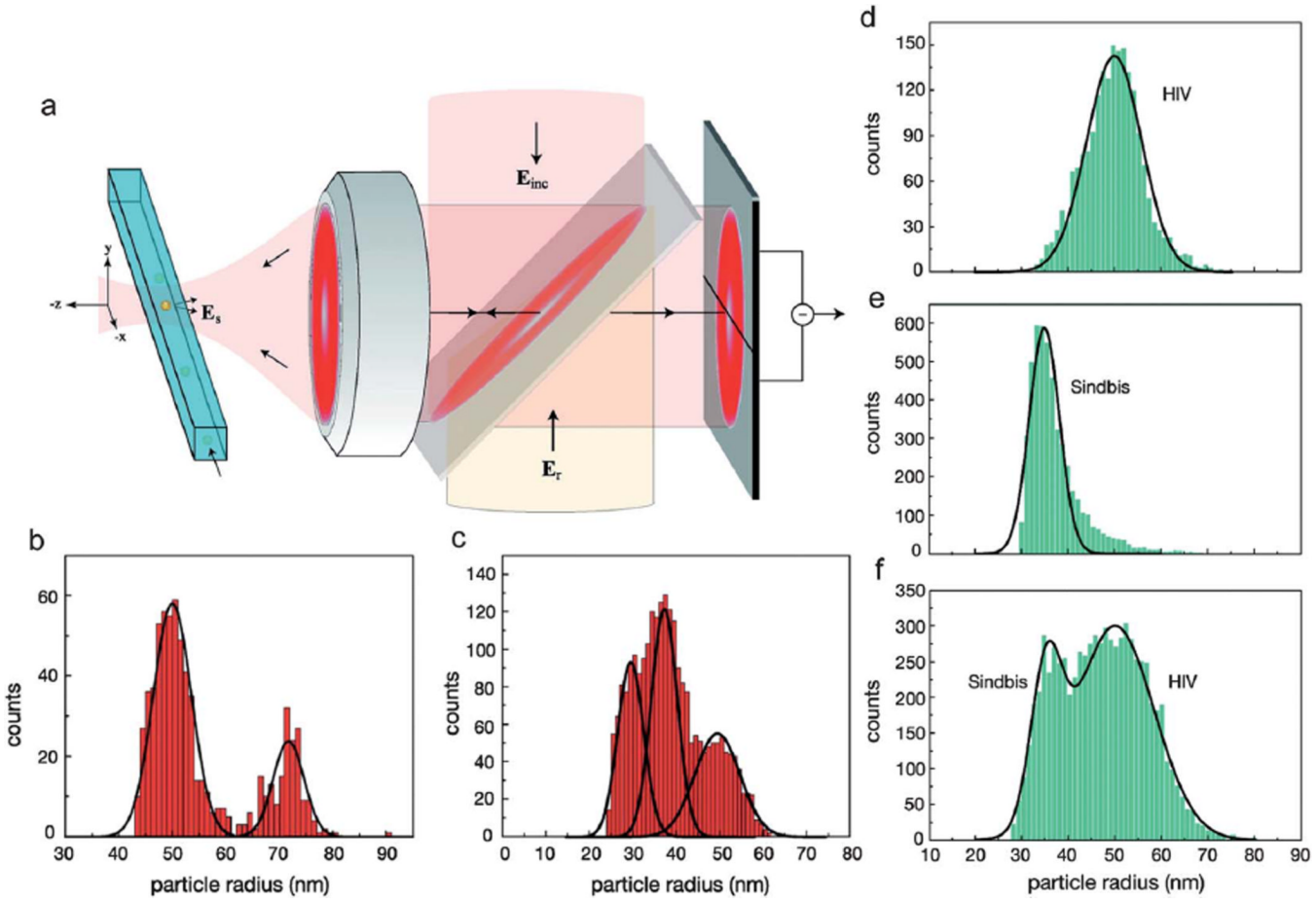

Fig. 5.

Flow-based Heterodyne Interferometric Detector. (a) Schematic of the heterodyne interferometric technique. The nanoparticle (yellow) is detected as it traverses the focused spot. The scheme employs an excitation laser (E_{exc}) with frequency that is reflected off a beamsplitter and focused *via* an objective into a nanofluidic channel. The scattered light (E_{sca}) from the nanoparticle is superimposed onto a reference beam (E_{ref}) with frequency ($\omega + \Delta\omega$) and directed onto a differential detector. (b) Particle size distributions for a mixture of 50 and 75 nm polystyrene nanoparticles. (c) Size distribution for a mixture of 30, 40, and 50 nm gold nanoparticles. Size distributions for (d) HIV (ADA strain) and (e) Sindbis virus. (f) Size distribution for a mixture of HIV and Sindbis viruses. Adapted from ref. 67. © 2010 American Chemical Society.

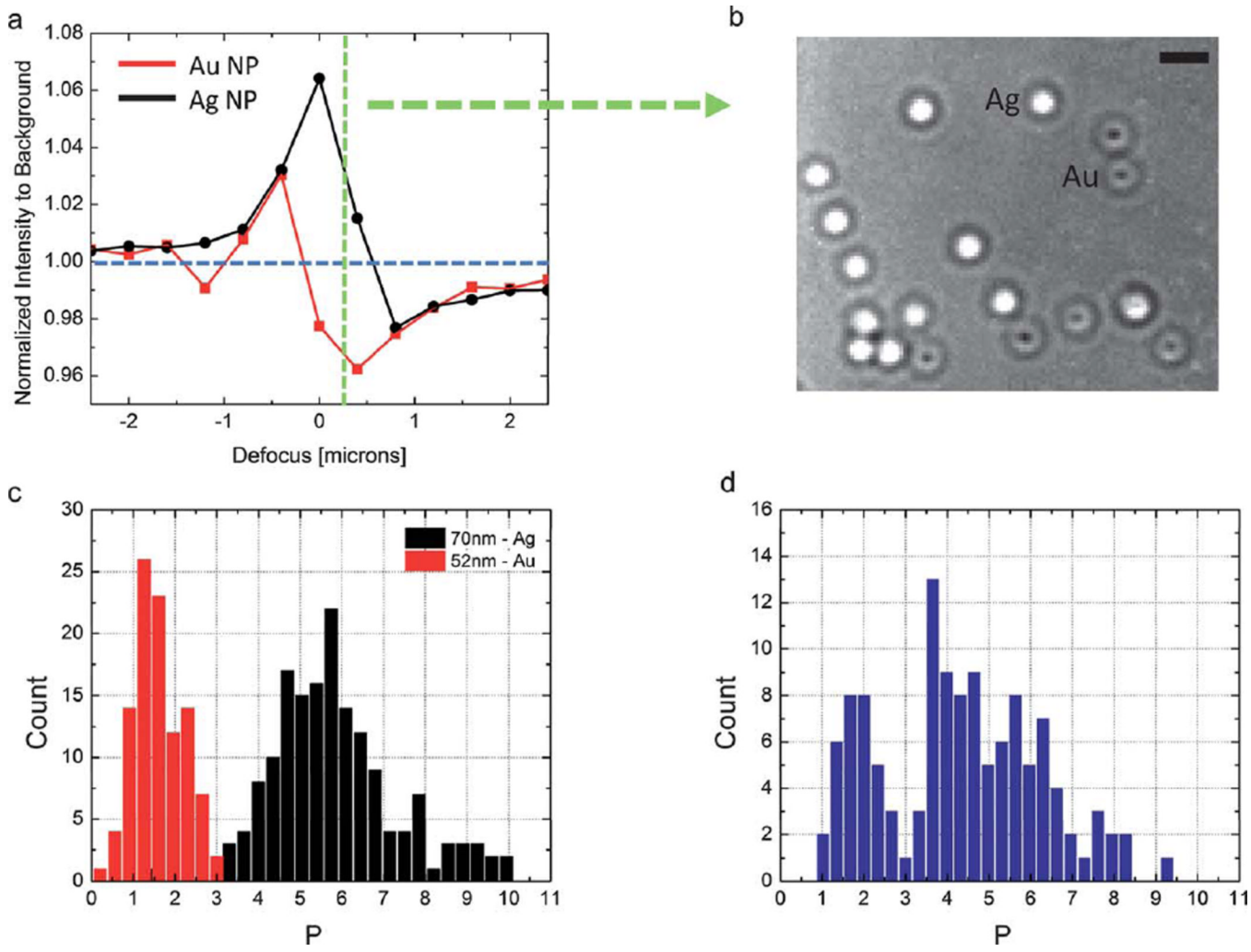

Fig. 6.

Material specific detection of nanoparticles using IRIS. (a) Background normalized peak response for 52 nm gold (red) and 70 nm silver (black) nanoparticles is shown as a function of defocus. (b) Interferometric image at 525 nm at a defocus of 250 nm. The scale bar denotes 2 micron. (c) High-throughput material based classification of 52 nm Au and 70 nm Ag particles. The measurements were done on separate chips. (d) Simultaneous detection of 52 nm Au and 70 nm Ag particles.

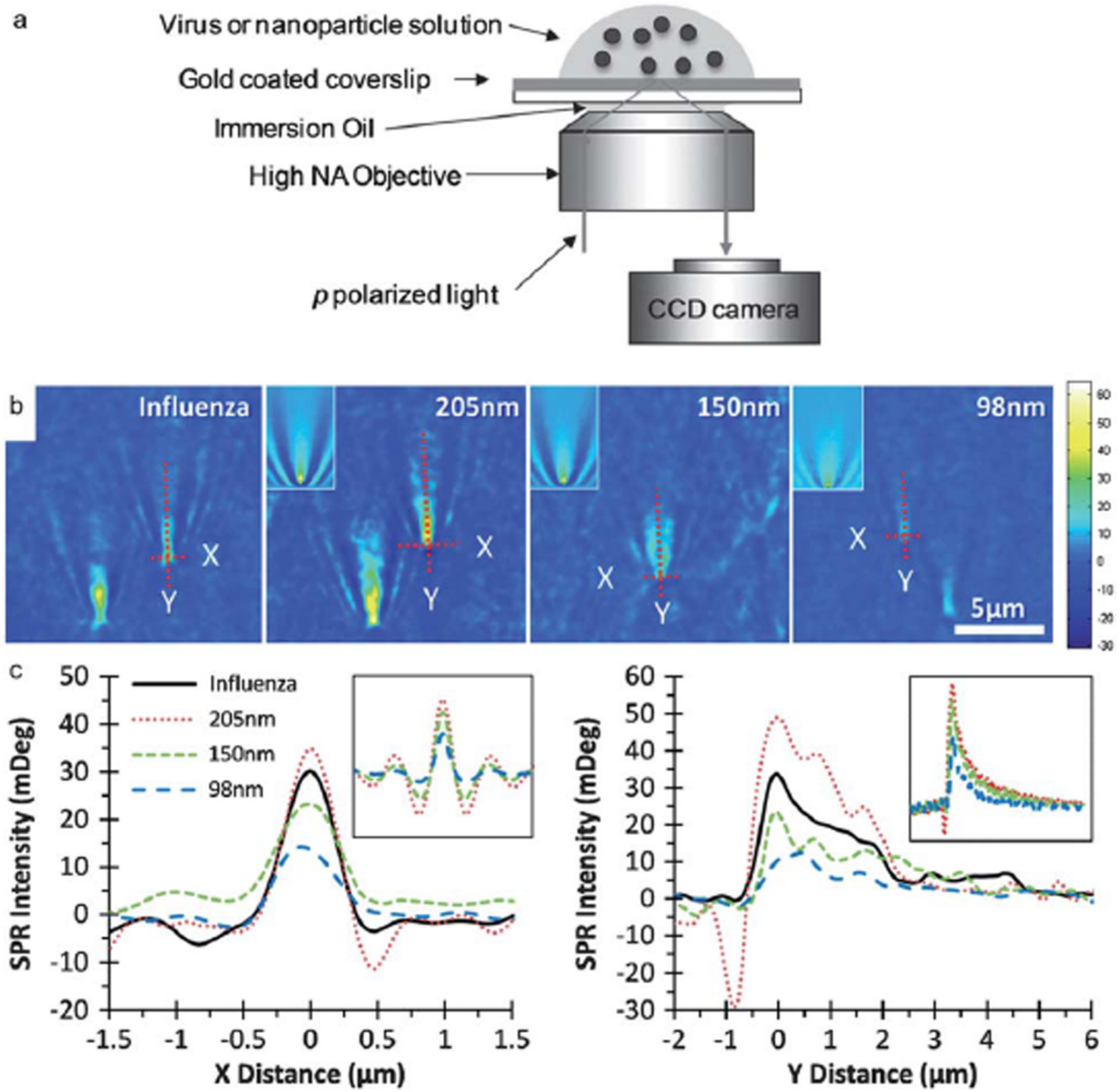

Fig. 7.

Surface Plasmon Resonance Microscopy (SPRM). (a) Schematic of the SPRM experimental setup. (b) SPRM images of H1N1 influenza A virus and three different silica nanoparticle populations in PBS buffer. For comparison with experiments insets in the images are nanoparticle images generated by numerical simulation. The SPR intensity profiles of selected particles along X (c) and Y (d) directions (indicated by dashed lines in (b)), respectively. The insets in the graph are the corresponding profiles from simulated images. Adapted from ref. 82. © 2010 National Academy of Sciences.

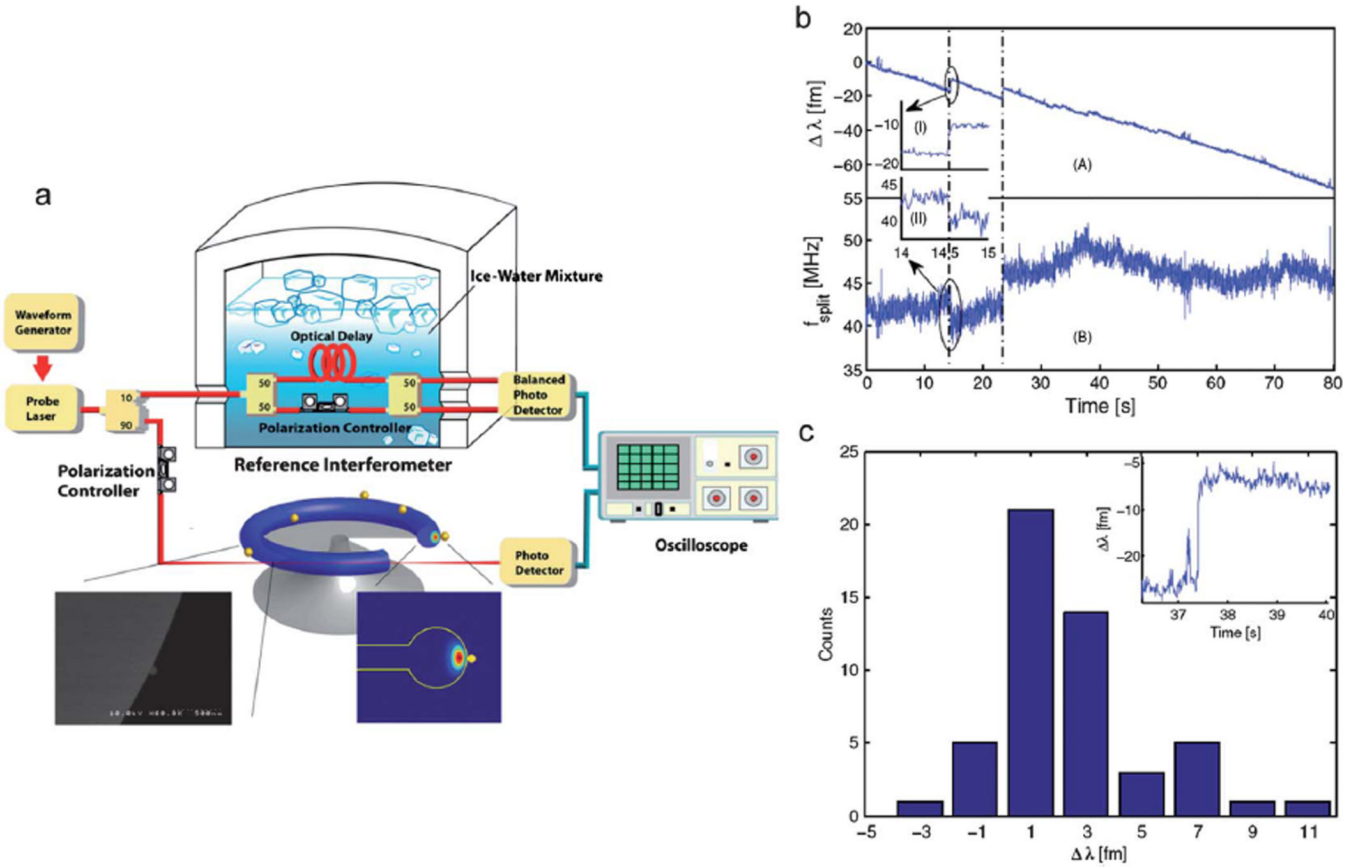

Fig. 8.

High Sensitivity Optical Microcavity based detector. (a) Experimental setup for nanoparticle detection using a temperature-stabilized reference interferometer. The output of a tunable laser is split into two branches by a 90/10 coupler. One branch is coupled into/out of a microtoroid resonator in a cooled aqueous environment. The other branch is coupled into a reference interferometer to monitor the laser optical frequency in real time. The reference interferometer is immersed in ice-water to improve the stability. (Inset) SEM micrograph of an $R = 25$ nm bead binding on the surface of a microtoroid. (b) The resonance wavelength shift (scan A) and splitting frequency shift (scan B) are shown for a microtoroid immersed in a 1 pMInfA solution. The insets I and II show that the same resonance wavelength shift event can also be detected as a split frequency shift, respectively. (c) The histogram of the resonance wavelength-shift steps in scan A and an inset of the largest wavelength step recorded of 11.3 fm. Adapted from ref. 99. © 2011 National Academy of Sciences.

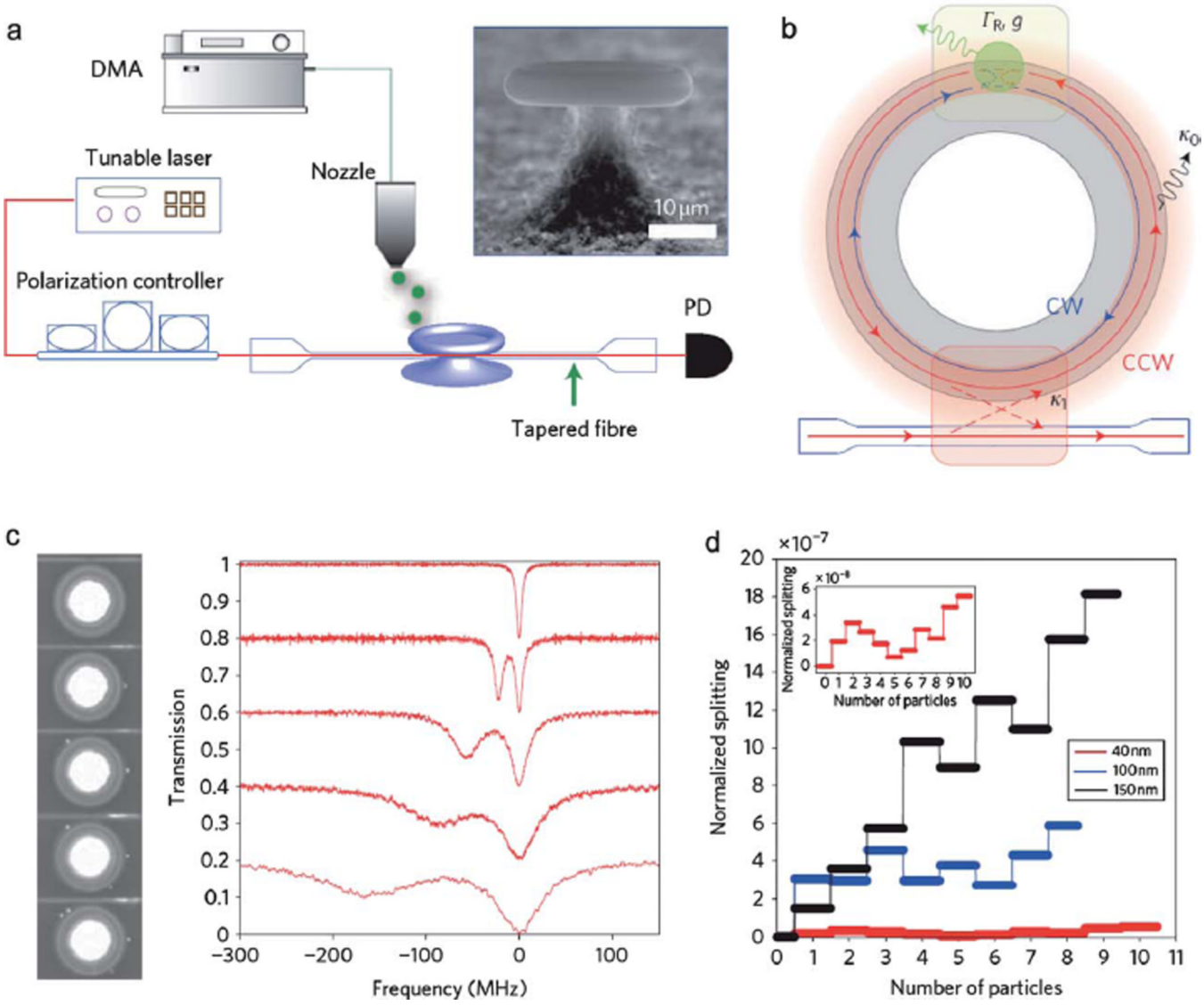

Fig. 9.

Mode splitting in an Ultrahigh-*Q* microresonator. (a) Schematic of the experimental setup. DMA, differential mobility analyser; PD, photo-diode. The inset shows an SEM image of a microtoroid. (b) Illustration of the coupled nanoparticle–microtoroid system. k_1, microtoroid–taper coupling rate; k_0, intrinsic damping rate (material and radiation losses); g, coupling coefficients of the light scattered into the resonator; GR, additional damping rate due to scattering losses. CW, clockwise modes; CCW, counter-clockwise modes. (c) Series of normalized transmission spectra taken at a 1550 nm wavelength band and the corresponding optical images recorded without nanoparticles (top trace) and with four successive depositions of KCl nanoparticles. The spectral baseline is vertically shifted for clarity. (d) Normalized splitting $2g/\omega_c$ ($2g$, splitting frequency; ω_c, resonance frequency) *versus* particle number for KCl nanoparticles. Each discrete step corresponds to a single nanoparticle binding event. The inset shows an enlarged plot for nanoparticles of $R = 40$ nm. Adapted from ref. 101. © 2010 Macmillan Publishers Ltd: Nature Photonics.